Preferred mitotic orientation in pattern formation by vascular mesenchymal cells

Margaret N. Wong, Timothy P. Nguyen, Ting-Hsuan Chen, Jeffrey J. Hsu, Xingjuan Zeng, Aman Saw, Eric M. Demer, Xin Zhao, Yin Tintut and Linda L. Demer

Am J Physiol Heart Circ Physiol 303:H1411-H1417, 2012. First published 12 October 2012;
doi: 10.1152/ajpheart.00625.2012

Am J Physiol Heart Circ Physiol 303: H1411–H1417, 2012.
First published October 12, 2012; doi:10.1152/ajpheart.00625.2012.

Preferred mitotic orientation in pattern formation by vascular mesenchymal cells

Margaret N. Wong,[1] Timothy P. Nguyen,[1] Ting-Hsuan Chen,[2] Jeffrey J. Hsu,[3] Xingjuan Zeng,[4] Aman Saw,[3] Eric M. Demer,[5] Xin Zhao,[4] Yin Tintut,[3] and Linda L. Demer[1,3,6]

[1]*Department of Bioengineering, University of California, Los Angeles, California;* [2]*Department of Mechanical and Aerospace Engineering, University of California, Los Angeles, California;* [3]*Department of Medicine, University of California, Los Angeles, California;* [4]*Institute of Robotics and Automatic Information System, Nankai University, Tianjin, China;* [5]*College of Creative Studies, University of California-Santa Barbara, Goleta, California; and* [6]*Department of Physiology, University of California, Los Angeles, California*

Submitted 20 August 2012; accepted in final form 9 October 2012

Wong MN, Nguyen TP, Chen T, Hsu JJ, Zeng X, Saw A, Demer EM, Zhao X, Tintut Y, Demer LL. Preferred mitotic orientation in pattern formation by vascular mesenchymal cells. *Am J Physiol Heart Circ Physiol* 303: H1411–H1417, 2012. First published October 12, 2012; doi:10.1152/ajpheart.00625.2012.—Cellular self-organization is essential to physiological tissue and organ development. We previously observed that vascular mesenchymal cells, a multipotent subpopulation of aortic smooth muscle cells, self-organize into macroscopic, periodic patterns in culture. The patterns are produced by cells gathering into raised aggregates in the shape of nodules or ridges. To determine whether these patterns are accounted for by an oriented pattern of cell divisions or postmitotic relocation of cells, we acquired time-lapse, videomicrographic phase-contrast, and fluorescence images during self-organization. Cell division events were analyzed for orientation of daughter cells in mitoses during separation and their angle relative to local cell alignment, and frequency distribution of the mitotic angles was analyzed by both histographic and bin-free statistical methods. Results showed a statistically significant preferential orientation of daughter cells along the axis of local cell alignment as early as *day 8*, just before aggregate formation. This alignment of mitotic axes was also statistically significant at the time of aggregate development (*day 11*) and after aggregate formation was complete (*day 15*). Treatment with the nonmuscle myosin II inhibitor, blebbistatin, attenuated alignment of mitotic orientation, whereas Rho kinase inhibition eliminated local cell alignment, suggesting a role for stress fiber orientation in this self-organization. Inhibition of cell division using mitomycin C reduced the macroscopic pattern formation. Time-lapse monitoring of individual cells expressing green fluorescent protein showed postmitotic movement of cells into neighboring aggregates. These findings suggest that polarization of mitoses and postmitotic migration of cells both contribute to self-organization into periodic, macroscopic patterns in vascular stem cells.

mitosis; vascular cells; reaction-diffusion; migration

IN THE EMBRYO, mitosis and cell movement are required for cells to self-organize into the complex patterns needed for shaping organs and tissues (2). Such self-organization requires coordination among cells that extends beyond immediate neighbors, often several cell diameters (10). In the adult, cellular self-organization is evidenced in vivo by alignment of smooth muscle cells around the artery wall and the graded orientation of layers of cardiac myocytes from endocardium to epicardium. In mutants lacking oriented cell division, kidney tubules grow by increasing diameter rather than length (6). Oriented cell division has a role in development of organ-shape definition (1). Hence, self-organization is significant in development and adult organ morphology.

Macroscopic pattern formation and self-organization have been shown to occur in cultured vascular cells in the form of evenly spaced aggregates that form stripe or spot patterns and that closely resemble, at the microscopic level, the atherosclerotic plaques found in the artery wall and on cardiac valve surfaces (8). Schor and colleagues (14) showed that vascular pericytes aggregate into raised, multicellular nodules that undergo coordinated contraction. Similar in vitro pattern formation occurs in vascular mesenchymal cells (VMCs; also known as calcifying vascular cells or vascular stem cells), which we isolated from bovine aortic smooth muscle cells by dilutional cloning (3). We further demonstrated that they have left-right chirality in migration (5) and the capacity to differentiate spontaneously along osteogenic, chondrogenic, myogenic, and marrow stromal lineages (19). Such multipotent vascular stem cells have been identified in vivo and may contribute to vascular remodeling and neointimal hyperplasia (17). However, it is unclear whether the macroscopic patterns of aggregates are formed by a local increase in mitotic activity or whether they are formed by oriented cell division. In the present study, we tested the relationship between mitotic orientation and local cell alignment, using phase-contrast and fluorescence time-lapse videomicrography with automated detection of the long axes of cells.

METHODS

Cell culture. VMCs were harvested, cultured, and passaged from bovine aortic media explants. Clones of VMCs were subcultured from these cells by dilutional cloning, as described previously (3, 20). We characterized these cells for expression of smooth muscle α-actin, calponin, caldesmon, myosin heavy chain, and antisurface ganglioside antibody 3G5, as described previously (3, 19). VMCs (*passages 15–21*) were grown in Dulbecco's modified Eagle's medium (DMEM) containing 15% heat-inactivated FBS (Hyclone) and supplemented with sodium pyruvate (1 mmol/l), penicillin (100 U/ml) and streptomycin (100 U/ml), all from Invitrogen or Irvine Scientific. For phase-contrast time-lapse experiments, cells were plated at 3×10^5 cells/well in 30-mm dishes. For inhibitor experiments, the cells from *passage 15* were plated at 5×10^4 cells/well in 24-well plates with 15% DMEM.

Time-lapse digital videomicroscopy. VMC cultures were incubated in a microscopic thermal stage (HCS60, Instec) at 37°C with a continuous supply of premixed 5% CO_2. Images of the 6 × 4.5-cm visual field were captured with a ×10 objective using a charge-coupled device (Coolsnap ES, Photometrics) along with an inverted phase-contrast microscope (Eclipse TE2000, Nikon). Time-lapse videomicroscopic imaging was initiated on *days 4* or *5* after plating,

Address for reprint requests and other correspondence: L. L. Demer, UCLA, Box 951679, Los Angeles, CA, 90095-1679 (e-mail: Ldemer@mednet.ucla.edu).

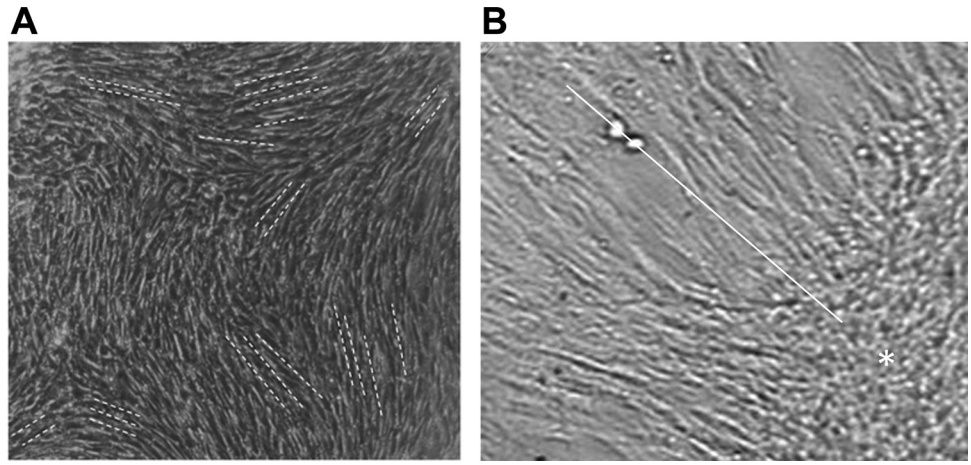

Fig. 1. Cell alignment. *A*: phase-contrast image of vascular mesenchymal cells (VMCs) at ~3 to 4 days in culture, showing swirling into regions of local alignment (near horizontal in *top* areas, near vertical in *bottom*, and diagonal at *middle*, as indicated by dashed lines). *B*: phase contrast image of VMC mitosis, showing alignment of mitotic axis (solid line determined by connecting the centers of the daughter cells) with the axis of local cell orientation. Both axes tend to orient toward the nearest forming aggregate (asterisk). Image width = 600 μm.

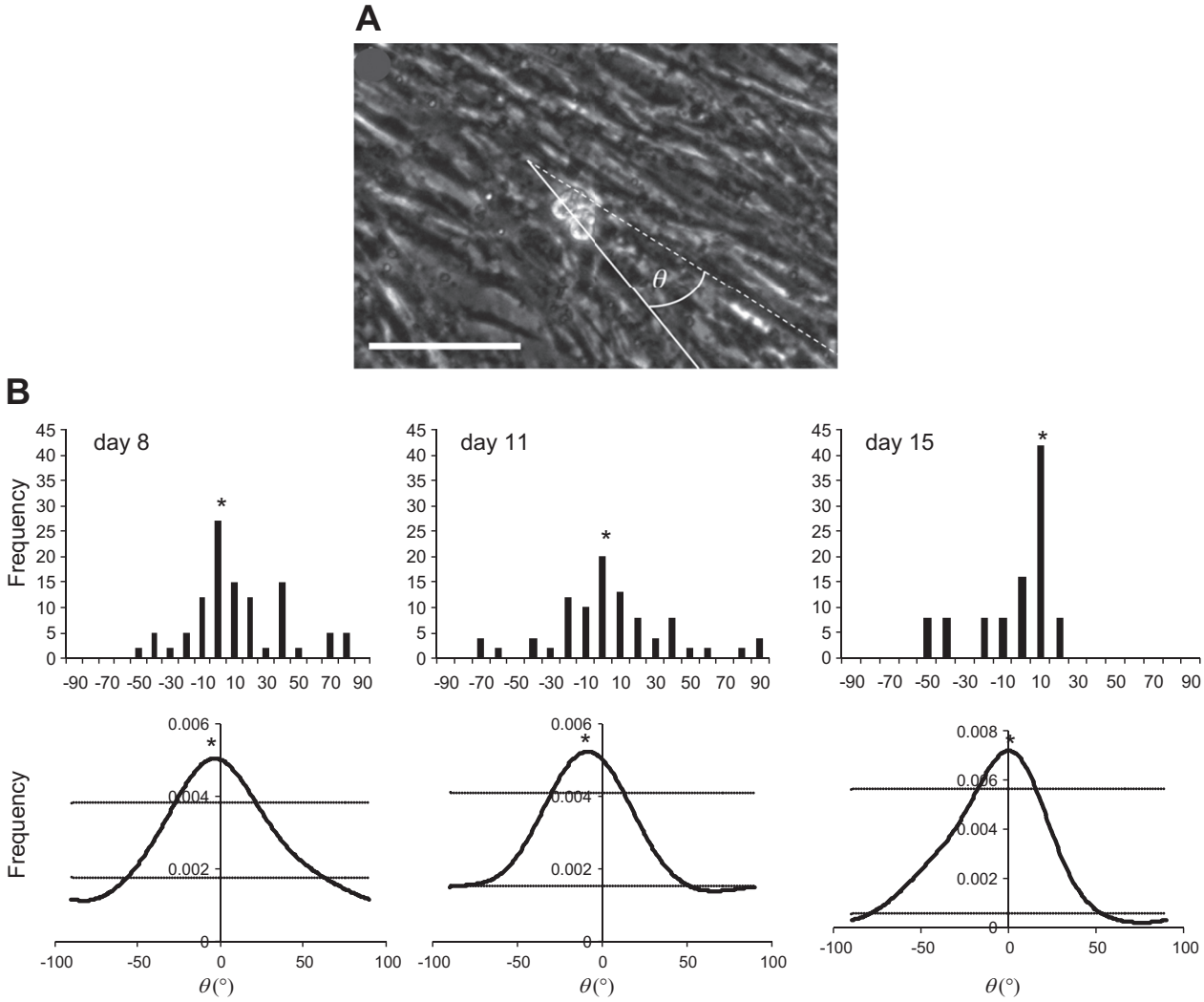

Fig. 2. Alignment of mitoses with one another and with local cell orientation. *A*: phase-contrast image of VMC culture (*day 8*) with superimposed schematic defining the mitotic separation angle θ, subtended by the local reference axis (dashed line), the prevailing orientation of local cell alignment, and the mitotic axis (solid line), defined by the line intersecting the center of two daughter cells from a given mitotic event. Scale bar = 100 μm. *B*: frequency histograms (*top*) and kernel density estimate distributions (*bottom*) of mitotic separation angle θ in VMC cultures. Horizontal lines in *B*, *bottom*, denote the upper 97.5 and lower 2.5% confidence bounds for the null hypothesis. Vertical axis units are probability/degree, and horizontal axis is mitotic angle measured in degrees. Statistical significance is indicated by the extension of the distribution curve above the upper line in all 3 panels. $*P < 0.025$.

Table 1. *Frequency table for the angle of mitotic axis*

Experiment	*Bin*	Given Angle Range, °	Expected Number of Cells/Angle-Interval Mean, 95% Confidence Interval	Observed Number of Cells/Angle Interval
I	*A*	1–36	4.6 (1.0–8.5)	1
	B	37–72	4.6 (1.0–8.7)	12*
	C	73–108	4.6 (1.0–8.7)	6
	D	109–144	4.6 (1.0–8.7)	1
	E	145–180	4.6 (1.0–8.5)	3
II	*A*	1–36	8.4 (3.7–13.7)	6
	B	37–72	8.4 (3.8–13.9)	17*
	C	73–108	8.4 (3.8–13.8)	10
	D	109–144	8.4 (3.9–13.8)	4
	E	145–180	8.4 (3.7–13.7)	5
III	*A*	1–36	6.0 (2.0–10.4)	4
	B	37–72	6.0 (2.0–10.6)	3
	C	73–108	6.0 (2.0–10.6)	2
	D	109–144	6.0 (2.0–10.6)	9
	E	145–180	6.0 (2.0–10.4)	12*

*Observed value outside the 95% confidence interval.

acquired every 5 min for 24–72 h, and repeated approximately every 3 days through *day 15*. The resulting images were saved as TIFF files and converted into an AVI file, using Windows Live Movie Maker.

Image analysis. The local reference axis was defined as the mean angle of individual cell long axes in a given region such as the area surrounding a given mitosis. Individual cell axes were determined by automated edge-detection software. After the image contrast was adjusted, the images were made binary and the cells were identified using size and intensity thresholds. The mitotic axis was defined as that intersecting the centers of the daughter cells (Fig. 1*B*). From these two axes, we defined the mitotic separation angle, θ, as that subtended by the reference and mitotic axes (Fig. 2*A*). Mitoses within aggregates were excluded because they lack local alignment. Additional analyses were performed to test whether mitotic alignment depends on presence of aggregates by separately analyzing mitoses that occurred before (*day 8*), during (*day 11*), and after (*day 15*) aggregate formation. For the remaining experiments using different clones and those with inhibitor treatments, multiple days were combined in the analysis.

Treatment. The nonmuscle myosin-II inhibitor blebbistatin (10 μM, Sigma-Aldrich, St. Louis, MO) and the Rho kinase inhibitor Y-27632 (10 μM, Ascent Scientific) were used to perturb cell mitotic organization. Mitomycin C (1 μg/ml; Sigma) was used to inhibit cell division. These inhibitors were added at the time of plating and replenished with each media change.

Transfection and fluorescence time-lapse videomicroscopic imaging. For experiments using green fluorescent protein (GFP), VMCs from *passage 20* were plated at 2×10^5 cells/well in 60-mm dishes with 15% DMEM. Approximately 1 μg of plasmid carrying GFP was transfected 1 day after plating using the Effectene transfection reagent (Qiagen, Valencia, CA) to achieve a transfection efficiency of 1–3% to allow tracking of single cells. The media were changed 24 h after transfection and every 3 to 4 days afterward. Time-lapse imaging in a humidity, CO_2, and temperature-controlled stage was started 11 days after plating and continued for 3 days. Three GFP-labeled cells were examined in this manner.

Statistical analysis. Results of the image analysis were first displayed as frequency histograms for θ in bins of 10° width for the mitoses recorded in each culture. For typical data, histogram-based methods suffer from artifacts because of the arbitrary nature of bin size and location. To eliminate these potential artifacts of binning, we assessed statistical significance of clustering using a bin-free approach, specifically, kernel density estimation (15). In this approach, many small elementary functions centered at the data values are used to build up a continuous estimate of the distribution of the data, which is independent of any bin-size choice. As the kernel functions, we used von Mises distributions, i.e., Gaussian distributions modified for circular or angular data. The width of the kernel functions was chosen to maximize the power of our statistical test against an equal mixture of the uniform distribution and the cosine distribution. For each data set, we estimated its probability density function and found its maximum and minimum values. These values were then compared with the maxima and minima of 50,000 similar curves constructed with similarly sized samples from the uniform distribution, using Monte Carlo simulation implemented in Python (routines available on request). If a maximum exceeded the 97.5th percentile of the simulated maxima or a minimum was less than the 2.5th percentile of the

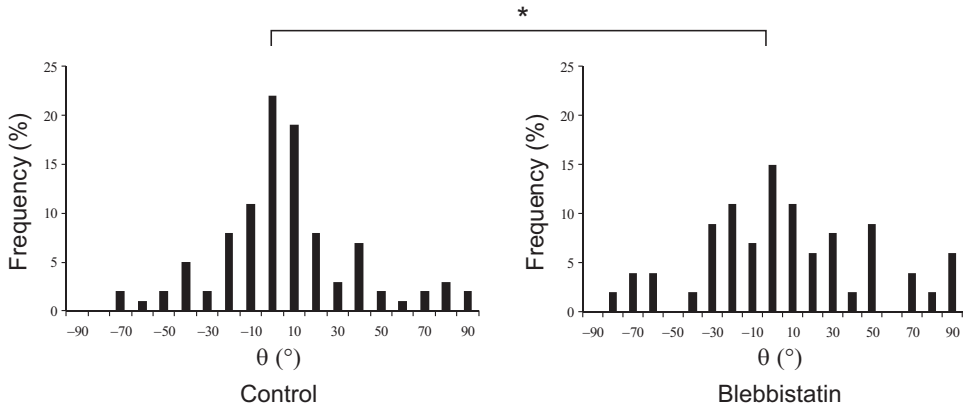

Fig. 3. Blebbistatin treatment. Frequency histograms for cells treated with control medium or blebbistatin (10 μM), including mitoses occurring from days *8–15*, showing significantly different indexes of dispersion for control vs. treated cultures (nonoverlapping 95% confidence intervals; $*P < 0.05$).

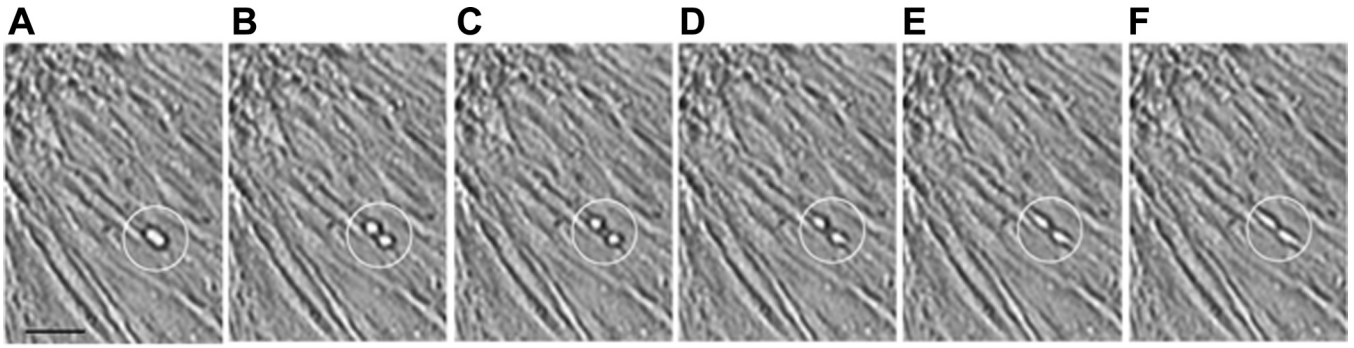

Fig. 4. Angle of daughter-cell migration. Phase-contrast, sequential, time-lapse, videomicrographic images from VMC cultures, showing representative mitotic events (circled) where daughter cells separate in opposite directions along an axis parallel to the mitotic separation angle and nearly parallel to the reference axis of local alignment. Scale bar = 100 μm.

simulated minima, we considered the deviation, i.e., the degree of clustering, to be statistically significant at the $P < 0.05$ level.

For comparison of treated versus untreated cultures, we used an index of dispersion (ID) (22), which is defined as the variance of bin counts divided by the mean bin count of a histogram. For data with low coherence (clustering), the index is $<<1$. For data with high coherence, the index was $>>1$. For data randomly distributed by a Poisson process, the index is ~1. To assess statistical significance of different indexes, we used resampling "bootstrap" analysis to determine confidence intervals. Each data set was randomly resampled 1,000 times, and the indexes of dispersion for the random samples were used to calculate 95% confidence intervals around the observed ID.

RESULTS

Cell alignment. At ~3 to 4 days in culture, VMCs showed local cell alignment in regions measuring ~2 × 2 cm. This local cell alignment, described using the local reference axis (dashed lines, Fig. 1*A*) was defined as the mean angle of individual cell axes in a given region, where individual cell axes were determined by automated edge-detection software. At ~2 wk after plating, cell divisions appeared to orient such that the line connecting daughter cells ("mitotic axis"; solid line, Fig. 1*B*) was typically parallel to the local cell alignment (supplemental video 1). Both the mitotic axis and the local reference axis were typically oriented toward the nearest aggregate (asterisk, Fig. 1*B*).

Alignment of mitotic axes with one another. To determine whether the mitoses within a given field of view were aligned with one another, we determined the angle of the mitotic axis relative to the edge of the field of view for each of 23 to 42 mitoses in time-lapse videomicroscopy. This was repeated in three different cultures from one clone. Results of the image analysis are displayed as a frequency table for the angle of the mitotic axis in bins of 36° width. By comparison with the expected number of cells per angle-interval for the theoretical case of completely random orientation, the observed numbers of cells per angle-interval showed statistically significant clustering for each of the three cultures ($*P < 0.05$; Table 1).

Alignment with local reference axes. To determine whether the mitotic axes aligned with the local reference axes, we determined θ (the angle separating the mitotic axis from the local reference axis; Fig. 2*A*) for 12–40 mitoses from time-lapse videomicroscopic images from two different cultures from a second clone. If the axes are in alignment, the values of θ should cluster around zero. To determine whether the clustering is statistically significant, we used a bin-free approach, kernel density estimation (15), to avoid artifacts because of choice of bin size and location. Data are displayed as both conventional histograms, using bins of 10° width, and Kernel Density Estimation distributions (Fig. 2*B*, *top* and *bottom*, respectively).

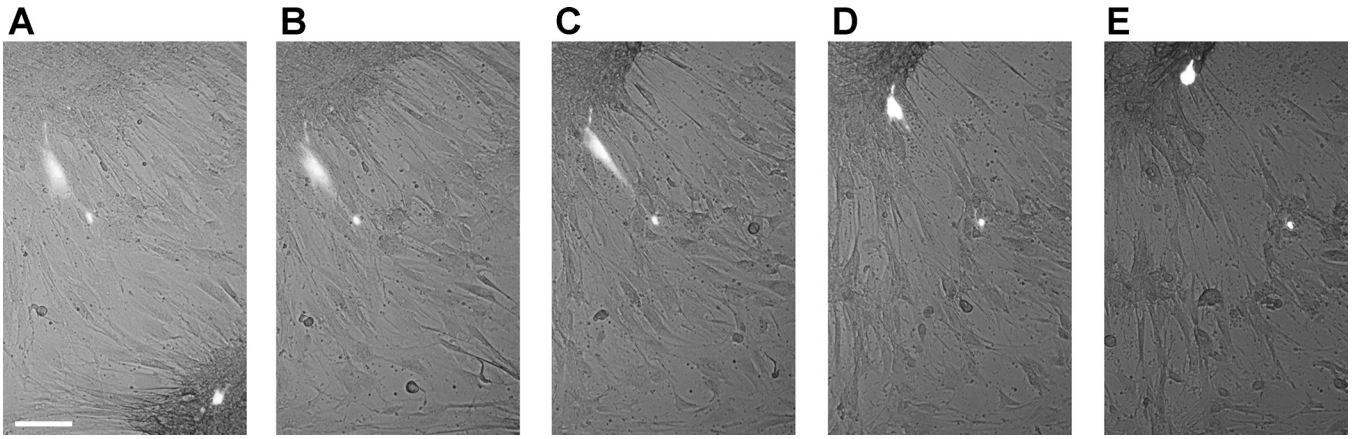

Fig. 5. Time-lapse, fluorescence microscopic images of VMCs expressing green fluorescent protein (GFP) at low efficiency. *A–E*: sequence showing two GFP-positive cells at 2 wk of culture. One GFP-positive cell (*bottom right corner*) is located within an aggregate that shifts out of the field of view in later images. The other GFP-positive cell migrates toward an aggregate (*top left corner*), leaving behind a cytoplasmic fragment. Scale bar = 100 μm.

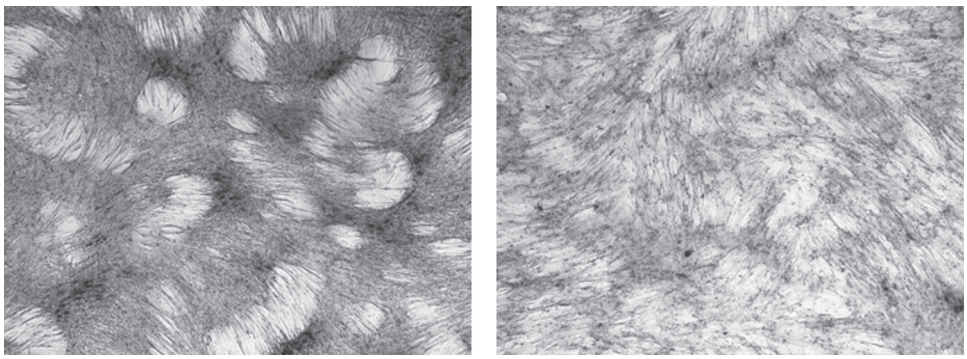

Fig. 6. Effect of mitosis inhibition on pattern formation. Light microscopic hematoxylin-stained images of VMCs treated with vehicle control (*left*) or mitomycin C (1 μg/ml, *right*) at *day 8*. Magnification, ×40.

Results showed that the clustering of θ values around zero (indicating alignment of mitotic axes with one another and with the local reference axis) was statistically significant at *day 8* ($n = 40$; $^*P < 0.025$; Fig. 2*B*, *left*). To determine whether the results were consistent over time in culture and whether they were dependent on presence of aggregates, we repeated the analysis on *days 11* and *15*, during which time aggregate formation occurs. Results showed that the clustering of θ values around zero was also statistically significant during aggregate formation (*day 11*; $n = 28$; $^*P < 0.025$; Fig. 2*B*, *middle*) and after aggregate formation (*day 15*; $n = 12$; $^*P < 0.025$; Fig. 2*B*, *right*), suggesting that the mitotic axes were aligned with one another and with the local reference axis.

Inhibition of stress fiber orientation. To assess whether the alignment of mitotic axes with each other and with the local reference axis was dependent on stress fiber orientation, we compared the findings with cells treated with the nonmuscle myosin II inhibitor, blebbistatin, or the Rho kinase inhibitor Y-27632 (21). For statistical comparison, we used an ID (22) that is defined as the variance of bin counts divided by the mean bin count of a histogram. For data with low clustering, the index is $<<1$. For data with high clustering, the index is $>>1$. Results showed that the ID was significantly greater in the control, pooled data than in cultures treated with blebbistatin [ID = 12.7; 95% confidence interval (7.6, 20.7) vs. 2.6; 95% confidence interval (1.4, 6.2)] (Fig. 3), suggesting a loss of mitotic alignment with blebbistatin treatment and a role for nonmuscle myosin II in the process. Cultures treated with Y-27632 exhibited no defined local cell alignment (data not shown, since θ is undefined in the absence of local alignment), suggesting a role for Rho kinase in self-organization of the cells in general.

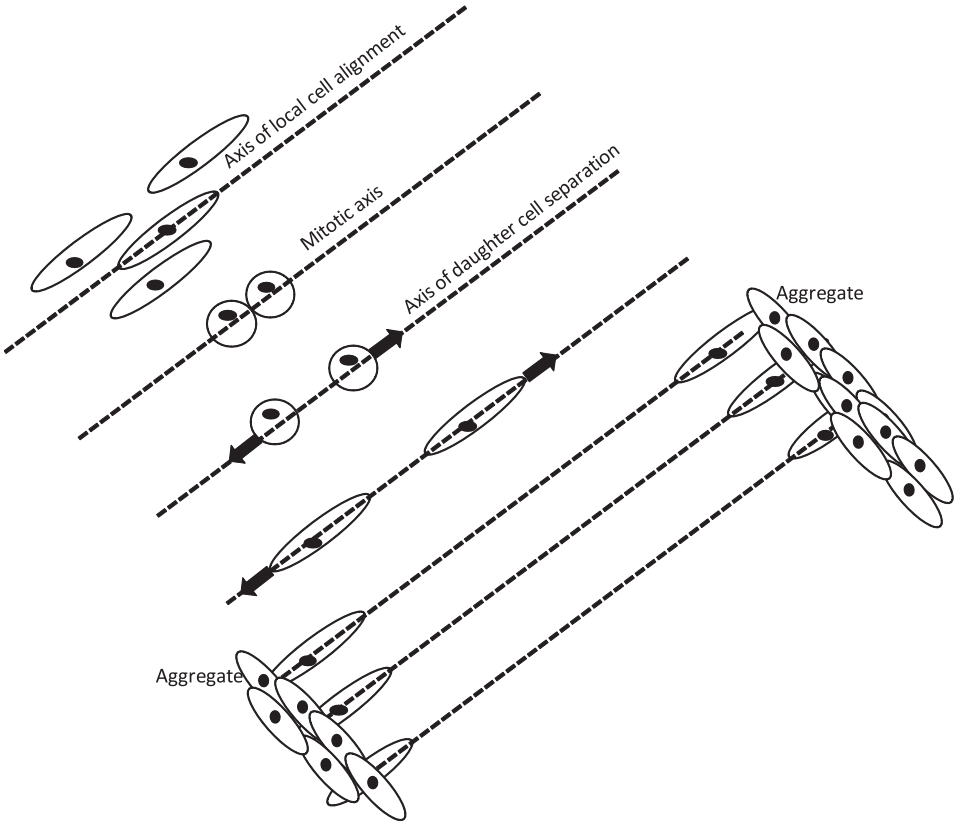

Fig. 7. Schematic diagram showing relationships between axes of local cell alignment, mitoses, daughter cell separation, and aggregates. In a given local domain, the long axes of cells tend to align in parallel with each other, forming an "axis of local cell alignment." Within the same domain, the mitoses are oriented in parallel with each other and with the axis of local cell alignment, forming a "mitotic axis." When the daughter cells separate, they tend to migrate apart along an "axis of daughter cell separation," parallel to the mitotic axis where they join cells from neighboring domains in aggregates.

Migration path. Following mitosis, the daughter cells were observed to migrate in opposite directions along the local reference axis (Fig. 4, *A–H*). Systematic analysis was not performed because the daughter cells quickly spread and lost phase-contrast refractility as they migrated. To observe migration of individual cells, we transfected a culture of VMCs with a plasmid carrying GFP at low transfection efficiency. By time-lapse fluorescence microscopy, we tracked a GFP-positive cell migrating to the edge of an aggregate, where it appeared to extend and slide into a thin cytoplasmic projection (Fig. 5; supplemental video 2). To determine whether the inhibition of mitosis affects cell migration, cells were continuously treated with the mitosis inhibitor mitomycin C (1 μg/ml). Since pattern formation occurs over days, a lower concentration of mitomycin C was used to avoid the toxicity seen with chronic treatment at higher concentration. This concentration partially blocked mitosis and partially blocked macroscopic pattern formation, suggesting that cell division contributes in part to the mechanism of self-organization of these cells (Fig. 6).

Altogether, these observations suggest that mitotic orientation is coordinated and aligned with local cell axes, raising the possibility that it contributes to self-organization of VMC into macroscopic patterns.

DISCUSSION

These findings indicate that when VMC divide, mitotic orientation is coherent within local domains (Fig. 7). This alignment correlates with the long axes of cells in that region, and the daughter cells separate along that same axis toward macroscopic aggregates. This aggregate formation is inhibited by blocking mitosis with mitomycin C.

Evidence supports an in vivo role for mitotic orientation in determining the shape of structures and/or organs. For example, mutations affecting orientation of cell division disrupt organ morphogenesis in drosophila, resulting in dysmorphic features, such as loss of wing elongation (1). Similarly, overduplication of centrosomes, which is likely to disrupt mitotic orientation, leads to formation of abnormal vasculature when induced by treatment with vascular endothelial growth factor (18). Our findings suggest that alignment of mitotic orientation underlies cellular self-organization by orienting daughter cells to migrate in a particular direction in a coordinated manner and that it contributes to the formation of periodic patterns of multicellular aggregates by organizing cell migration. This raises the possibility that local disruption of mitotic alignment may mitigate pathological forms of cellular aggregation, such as nodules in calcific aortic valve stenosis.

In our studies, the alignment of mitotic orientation persisted, though somewhat diminished, with inhibition of nonmuscle myosin-II kinase, suggesting a small role of for this factor. The diminished pattern formation with mitomycin C-induced mitotic arrest suggests a role of cell division in self-organization, although we cannot exclude the possibility that cell density confounded this result. The finding that alignment remains consistent before, during, and after aggregate formation suggests that contraction of mature aggregates is not required. However, it remains possible that synchronized contraction and extracellular matrix wrinkling occur before distinct aggregates are visible.

A number of mechanisms may explain oriented cell division. Pattern formation in VMCs and other cells appears to be governed by reaction-diffusion phenomena that provide chemical gradients in prepatterns in embryonic tissue formation (4, 7, 9, 16). Chemical gradients also drive cell alignment as in Drosophila (11). Mechanical factors, such as the cell traction phenomenon (12), substrate interfaces (5), and cell chirality (13), may also contribute. In the cell traction phenomenon, extracellular matrix is deformed by the traction forces of motile cells, and this anisotropic "wrinkling" guides cell movements in a preferred direction, as wheels in "ruts." Overall, these findings suggest that nonrandom orientation of mitoses, alignment of mitotic orientation with local cell alignment, and postmitotic migration may all contribute to the formation of macroscopic periodic patterns in vascular cells.

Overall, these findings are relevant to disease in that this culture model may be used to study atherosclerotic plaque, such as determinants of mechanical vulnerability. They also may provide an in vitro model for developmental embryogenesis, allowing study of the mechanisms driving cellular self-organization required for embryogenesis. In addition, the findings are relevant to tissue regeneration engineering, because they add to our fundamental understanding of cellular self-organization and provide a potential approach for coaxing cells into macrostructures that recapitulate the architecture of normal tissues.

ACKNOWLEDGMENTS

We are grateful to Dr. Chih-Ming Ho for the use of imaging facilities.

GRANTS

This research was supported in part by National Heart, Lung, and Blood Institute Grant HL-081202 (to L. L. Demer and Y. Tintut), National Science Foundation Grant EFRI-1025073 (to L. L. Demer), and the Laubisch Endowment at University of California, Los Angeles.

DISCLOSURES

No conflicts of interest, financial or otherwise, are declared by the author(s).

AUTHOR CONTRIBUTIONS

M.N.W., T.P.N., T.-H.C., A.S., Y.T., and L.L.D. conception and design of research; M.N.W., T.P.N., T.-H.C., J.J.H., A.S., Y.T., and L.L.D. performed experiments; M.N.W., T.P.N., T.-H.C., J.J.H., X. Zeng, A.S., E.M.D., X. Zhao, Y.T., and L.L.D. analyzed data; M.N.W., T.P.N., T.-H.C., J.J.H., X. Zeng, E.M.D., X. Zhao, Y.T., and L.L.D. interpreted results of experiments; M.N.W., T.P.N., A.S., E.M.D., X. Zhao, Y.T., and L.L.D. prepared figures; M.N.W., T.P.N., T.-H.C., J.J.H., X. Zeng, E.M.D., X. Zhao, Y.T., and L.L.D. edited and revised manuscript; M.N.W., T.P.N., T.-H.C., J.J.H., X. Zeng, A.S., E.M.D., X. Zhao, Y.T., and L.L.D. approved final version of manuscript; L.L.D. drafted manuscript.

REFERENCES

1. **Baena-Lopez LA, Baonza A, Garcia-Bellido A.** The orientation of cell divisions determines the shape of Drosophila organs. *Curr Biol* 15: 1640–1644, 2005.
2. **Bischoff M, Cseresnyes Z.** Cell rearrangements, cell divisions and cell death in a migrating epithelial sheet in the abdomen of Drosophila. *Development* 136: 2403–2411, 2009.
3. **Bostrom K, Watson KE, Horn S, Wortham C, Herman IM, Demer LL.** Bone morphogenetic protein expression in human atherosclerotic lesions. *J Clin Invest* 91: 1800–1809, 1993.
4. **Chen TH, Guo C, Zhao X, Yao Y, Bostrom KI, Wong MN, Tintut Y, Demer LL, Ho CM, Garfinkel A.** Patterns of periodic holes created by increased cell motility. *Interface Focus* 2: 457–464, 2012.
5. **Chen TH, Hsu JJ, Zhao X, Guo C, Wong MN, Huang Y, Li Z, Garfinkel A, Ho CM, Tintut Y, Demer LL.** Left-right symmetry break-

ing in tissue morphogenesis via cytoskeletal mechanics. *Circ Res* 110: 551–559, 2012.
6. **Costantini F, Kopan R.** Patterning a complex organ: branching morphogenesis and nephron segmentation in kidney development. *Dev Cell* 18: 698–712, 2010.
7. **Garfinkel A, Tintut Y, Petrasek D, Bostrom K, Demer LL.** Pattern formation by vascular mesenchymal cells. *Proc Natl Acad Sci USA* 101: 9247–9250, 2004.
8. **Gimbrone MA Jr, Cotran RS.** Human vascular smooth muscle in culture. Growth and ultrastructure. *Lab Invest* 33: 16–27, 1975.
9. **Harris AK, Stopak D, Warner P.** Generation of spatially periodic patterns by a mechanical instability: a mechanical alternative to the Turing model. *J Embryol Exp Morphol* 80: 1–20, 1984.
10. **Junkin M, Leung SL, Whitman S, Gregorio CC, Wong PK.** Cellular self-organization by autocatalytic alignment feedback. *J Cell Sci* 124: 4213–4220, 2011.
11. **Lawrence PA, Casal J, Struhl G.** The hedgehog morphogen and gradients of cell affinity in the abdomen of Drosophila. *Development* 126: 2441–2449, 1999.
12. **Murray JD, Oster GF.** Cell traction models for generating pattern and form in morphogenesis. *J Math Biol* 19: 265–279, 1984.
13. **Pohl C, Bao Z.** Chiral forces organize left-right patterning in *C. elegans* by uncoupling midline and anteroposterior axis. *Dev Cell* 19: 402–412, 2010.
14. **Schor AM, Allen TD, Canfield AE, Sloan P, Schor SL.** Pericytes derived from the retinal microvasculature undergo calcification in vitro. *J Cell Sci* 97: 449–461, 1990.
15. **Scott DW.** *Multivariate Density Estimation, Theory, Practice, and Visualization*. Hoboken, NJ: Wiley & Sons, 1992.
16. **Sick S, Reinker S, Timmer J, Schlake T.** WNT and DKK determine hair follicle spacing through a reaction-diffusion mechanism. *Science* 314: 1447–1450, 2006.
17. **Tang Z, Wang A, Yuan F, Yan Z, Liu B, Chu JS, Helms JA, Li S.** Differentiation of multipotent vascular stem cells contributes to vascular diseases. *Nat Commun* 3: 875, 2012.
18. **Taylor SM, Nevis KR, Park HL, Rogers GC, Rogers SL, Cook JG, Bautch VL.** Angiogenic factor signaling regulates centrosome duplication in endothelial cells of developing blood vessels. *Blood* 116: 3108–3117, 2010.
19. **Tintut Y, Alfonso Z, Saini T, Radcliff K, Watson K, Bostrom K, Demer LL.** Multilineage potential of cells from the artery wall. *Circulation* 108: 2505–2510, 2003.
20. **Tintut Y, Parhami F, Bostrom K, Jackson SM, Demer LL.** cAMP stimulates osteoblast-like differentiation of calcifying vascular cells. Potential signaling pathway for vascular calcification. *J Biol Chem* 273: 7547–7553, 1998.
21. **Totsukawa G, Wu Y, Sasaki Y, Hartshorne DJ, Yamakita Y, Yamashiro S, Matsumura F.** Distinct roles of MLCK and ROCK in the regulation of membrane protrusions and focal adhesion dynamics during cell migration of fibroblasts. *J Cell Biol* 164: 427–439, 2004.
22. **Upton G, Cook I.** *A Dictionary of Statistics*. Oxford, UK: Oxford University Press, 2006.